

# Rethinking Molecule Synthesizability with Chain-of-Reaction

Seul Lee<sup>2\*</sup>, Karsten Kreis<sup>1</sup>, Srimukh Prasad Veccham<sup>1</sup>, Meng Liu<sup>1</sup>, Danny Reidenbach<sup>1</sup>, Saeed Paliwal<sup>1</sup>, Weili Nie<sup>1†</sup>, Arash Vahdat<sup>1†</sup>

<sup>1</sup> NVIDIA <sup>2</sup> KAIST

**Abstract:** A well-known pitfall of molecular generative models is that they are not guaranteed to generate synthesizable molecules. There have been considerable attempts to address this problem, but given the exponentially large combinatorial space of synthesizable molecules, existing methods have shown limited coverage of the space and poor molecular optimization performance. To tackle these problems, we introduce ReaSyn, a generative framework for synthesizable projection where the model explores the neighborhood of given molecules in the synthesizable space by generating pathways that result in synthesizable analogs. To fully utilize the chemical knowledge contained in the synthetic pathways, we propose a novel perspective that views synthetic pathways akin to reasoning paths in large language models (LLMs). Specifically, inspired by chain-of-thought (CoT) reasoning in LLMs, we introduce the chain-of-reaction (CoR) notation that explicitly states reactants, reaction types, and intermediate products for each step in a pathway. With the CoR notation, ReaSyn can get dense supervision in every reaction step to explicitly learn chemical reaction rules during supervised training and perform step-by-step reasoning. In addition, to further enhance the reasoning capability of ReaSyn, we propose reinforcement learning (RL)-based finetuning and goal-directed test-time compute scaling tailored for synthesizable projection. ReaSyn achieves the highest reconstruction rate and pathway diversity in synthesizable molecule reconstruction and the highest optimization performance in synthesizable goal-directed molecular optimization, and significantly outperforms previous synthesizable projection methods in synthesizable hit expansion. These results highlight ReaSyn’s superior ability to navigate combinatorially-large synthesizable chemical space.

## 1. Introduction

Discovering molecules with desired properties in the chemical space comprises the core of drug discovery. However, drug discovery pipelines are often very challenging and labor-intensive due to their vast design space and multi-objective nature. Molecular generative models have recently emerged as a notable breakthrough with the potential to greatly accelerate the drug discovery process. While promising, the practical impact of molecular generative models has remained limited as they share a common problem: generated drug candidates are often synthetically inaccessible [13, 51].

This problem arises from neglecting synthesizability during multi-objective molecular optimization, which often leads to exploration outside the synthesizable chemical space. A common strategy to alleviate this issue is to incorporate synthesizability as an additional optimization objective by quantitatively estimating synthesizability [11, 5, 48]. However, this approach is largely impractical since the heuristic synthesizability scores are far from reasonable proxies, as synthesizability is non-linear with structural changes and they cannot take available building block stocks or reaction selectivity into account [13]. An alternative approach is to constrain the design space to those that are synthetically accessible [47, 27, 7, 42], but existing methods that take this approach commonly sacrifice explorability, optimization performance, and controllability in the synthesizable chemical space.

A more effective strategy for synthesizable molecule design is to *project* molecules into the synthesizable space [14, 36, 46, 16]. In this strategy, often called synthesizable projection or synthesizable analog generation, a model learns to correct unsynthesizable molecules by generating synthetic pathways that lead to synthesizable analogs that are structurally similar to given molecules, thereby ensuring synthesizability under predefined sets of reactions and building blocks. This strategy benefit from its versatile and modular nature and can be used with any off-the-shelf molecular generative method to improve its practicality in real-world drug discovery. It can also be applied to explore neighborhoods in the synthesizable space, allowing the model to perform hit expansion or lead optimization. However, existing methods for synthesizable analog generation do not fully utilize the information from the chemical reactions in synthetic pathways and have shown limited coverage of synthesizable space, as observed in the low reconstruction rates of synthesizable molecules [3, 14, 36, 16]. While reactants, a reaction rule, and a product together define a chemical reaction, previous methods consider only some of these key components by omitting intermediate product molecules or reaction rules in synthetic

\* Work done during an internship at NVIDIA. <sup>†</sup> Equal advising.  
© 2025 NVIDIA. All rights reserved.

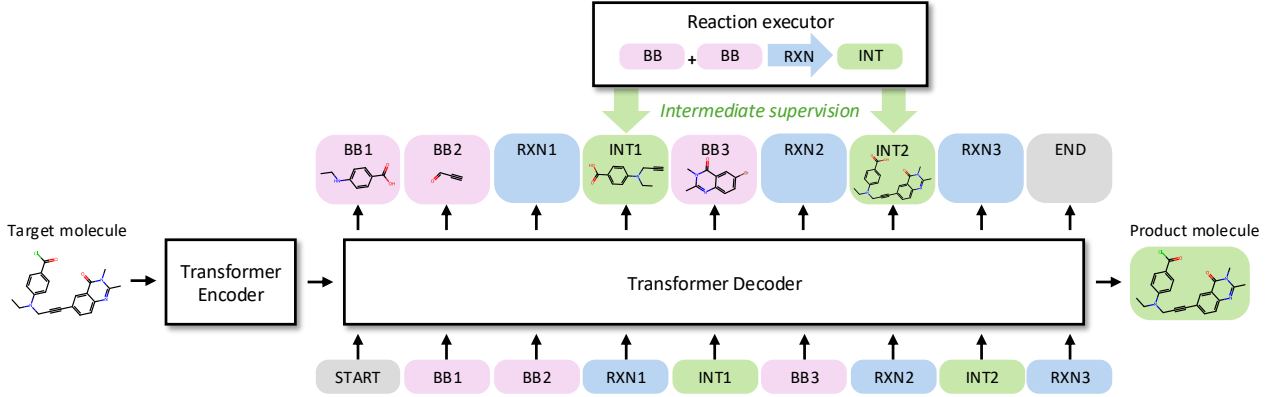


Figure 1 | The overall framework of ReaSyn. ReaSyn adopts an encoder-decoder Transformer architecture. After the Transformer encoder encodes the given target molecule, the Transformer decoder autoregressively predicts the synthetic pathways of its synthesizable analog in the CoR notation. ReaSyn has access to a reaction executor that yields the intermediate products with the predicted building blocks and reaction type. The CoR notation provides the model intermediate supervision during training and extra reasoning during inference.

pathways, i.e., they show insufficient reasoning capability on their synthetic pathways.

To tackle these limitations, we introduce ReaSyn<sup>1</sup>, a framework for effective synthesizable molecular projection with reasoning (Figure 1). Motivated by recent advances in large language model (LLM) reasoning, ReaSyn employs step-by-step thinking akin to chain-of-thought (CoT) reasoning [53], where each step is a single reaction in a multi-step synthetic pathway. Specifically, ReaSyn utilizes the *chain-of-reaction (CoR) notation* of synthesis where a full synthetic pathway is represented as a sequence that contains information of reactants, reaction type, and intermediate products of each reaction step as its subsequences (Figure 2(b)). Used in conjunction with autoregressive modeling with a Transformer architecture [50], the proposed CoR notation essentially views synthetic pathways as CoT reasoning paths of an LLM. Unlike previous synthetic pathway representations, our CoR notation explicitly incorporates the knowledge on step-by-step reaction rules by directly including intermediate molecules obtained from an external reaction executor, such as the RDKit library [29]. By imposing extra supervision on these intermediate molecules, the model can explicitly learn the chemical rules with richer supervision signals. Moreover, viewing synthetic pathway generation as LLM reasoning, the CoR notation also allows us to adopt techniques from LLM reasoning such as outcome-based reinforcement learning (RL) finetuning and test-time compute scaling, which we tailor here for improved synthesizable projection with ReaSyn.

We experimentally validate the effectiveness and versatility of ReaSyn on various tasks including synthesizable molecule reconstruction, synthesizable goal-directed molecular optimization, and synthesizable hit expansion. ReaSyn outperforms existing methods with superior reconstruction rate and pathway diversity in synthesizable molecule reconstruction, and achieves state-of-the-art performance in finding synthesizable chemical optima in synthesizable goal-directed molecular optimization and hit expansion. All these results indicate that ReaSyn has broader coverage and powerful explorability of the synthesizable chemical space, highlighting its efficacy as a practical tool in real-world drug discovery scenarios. We summarize our contributions as follows:

- We propose ReaSyn, a framework for synthesizable projection that uses the CoR notation of synthesis to view synthetic pathways as CoT reasoning paths.
- We propose RL finetuning and test-time compute scaling schemes tailored for projecting molecules into the synthesizable space to further enhance the performance of ReaSyn.
- We demonstrate the effectiveness and versatility of ReaSyn in various synthesizable molecule generation and optimization tasks through extensive experiments.

<sup>1</sup>Inspired of the reasoning nature of our problem, ReaSyn is pronounced similar to “reason”.

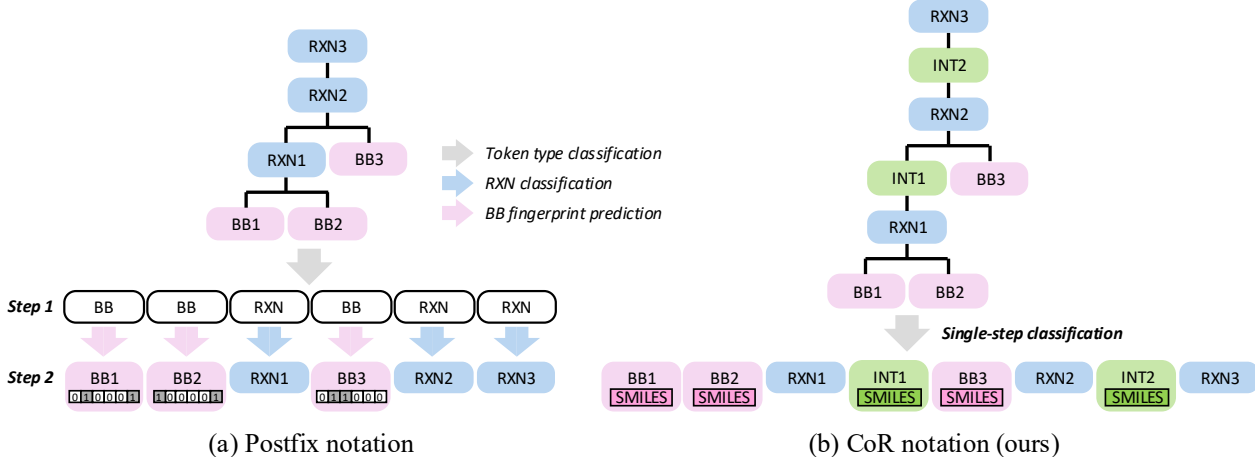


**Figure 2 | Comparison of the postfix notation and the CoR notation.** [START] and [END] tokens are omitted for simplicity. The postfix notation [36, 16] represents a synthetic pathway with a bi-level sequence consists of the token type level and the token feature level (the Morgan fingerprints for [BB] tokens and the reaction class for [RXN] tokens). Consequently, the synthetic pathways are embedded and generated in a hierarchical way in each autoregressive step. In contrast, the proposed CoR notation considers synthetic pathways as CoT reasoning paths by explicitly incorporating intermediate product molecules and removing the need for hierarchical classification.

## 2. Related Work

**Synthesizable molecule design.** Molecular synthesizability is a vital problem in drug discovery and therefore has received a lot of attention. In synthesizable molecule design, the synthesizable chemical space is defined by sets of reaction rules and building blocks, and the design space is constrained to this space. Various algorithms have been proposed to navigate the space to find synthesizable drug candidates, including variational autoencoders (VAEs) [39], Bayesian optimization [26], genetic algorithms (GAs) [14], Monte Carlo tree search (MCTS) [47], and GFlowNets [27, 42, 7]. However, they are either only capable of considering single-step synthetic pathways [39] or require extensive oracle calls to perform goal-directed molecular optimization [47, 27, 7, 42]. Furthermore, these *de novo* generation methods that aim to directly generate molecules in the synthesizable space exhibit poor explorability and optimization performance against the target chemical properties. An alternative approach is projecting given molecules into the synthesizable space to suggest synthesizable analogs [14, 36, 46, 16]. However, these methods are unable to reliably suggest synthetic pathways that reconstruct synthesizable molecules, have low pathway diversity, or show poor optimization performance. All of these results indicate a lack of explorability in the synthesizable chemical space, largely due to their insufficient reasoning capability on the generated synthetic pathways. On the other hand, a related but distinct area is retrosynthesis planning, which aims to predict synthetic pathways of given synthesizable molecules [6, 18, 25]. However, unlike the synthesizable projection approach, it cannot suggest synthesizable analogs given unsynthesizable molecules. In addition, since retrosynthesis planning is typically performed by a combination of a single-step reaction prediction model and a search algorithm, it cannot consider the entire pathway to further optimize the end products for target chemical property.

**Chain-of-thought in LLM reasoning.** Chain-of-thought (CoT) [53] is a strategy to explicitly incorporate reasoning steps before generating a final answer to a given question. Through step-by-step generation, CoT significantly improves reasoning capabilities and overall quality of generation of LLMs. With a dataset of question and CoT pairs, supervised finetuning (SFT) [35, 52, 49, 43, 21] can be applied to learn CoT generation. Another popular approach is LLM self-training via RL [20, 9, 40, 44, 49, 56, 43, 21]. Unlike SFT that usually utilizes one CoT reasoning path for each question, RL finetuning allows the model to discover multiple reasoning paths to a given question. On the other hand, reasoning with CoT can also be aided by external reasoning modules, such as using web searches to provide information for LLM-based multi-step research [38], or finetuning LLMs to call a calculator in mathematical formula generation [4].

**Test-time compute scaling in LLM reasoning.** Test-time compute scaling is a technique that enables LLMs to use additional computation at test-time. As reasoning requires making use of existing knowledge, test-time compute scaling has been considered as an effective strategy to improve reasoning capability and generation quality. The simplest such method is best-of-N sampling that generates multiple samples in parallel and select the best one using a verifier [4]. This approach can be improved by using a process reward model (PRM), which provides denser reward signals by scoring intermediate reasoning steps, not just the final answer [31]. Alternatively, more advanced approaches adopted search algorithms in LLM inference, and utilized a PRM to guide the search [55, 12].

### 3. Method

#### 3.1. Preliminaries

**Problem definition.** A set of building blocks  $\mathcal{B}$  and a set of reactions  $\mathcal{R}$  together define a *synthesizable chemical space*. A reaction  $R \in \mathcal{R}$  is a function that maps reactants to a product, and the synthesizable space  $\mathcal{C}$  is defined as the reachable product molecules by iterative application of the reactions in  $\mathcal{R}$  to possible combinations of the building blocks in  $\mathcal{B}$ . In our paper, "reactant" is defined as a molecule on which a reaction is performed, while "building block" is defined as a molecule that must be taken as a starting reactant for a synthetic pathway to be considered accessible. In practice, a reaction rule is described by SMILES Arbitrary Target Specification (SMARTS) [8], a regular expression-like representation for molecular patterns of reactants and products. A single reaction step is defined by executing a reaction to convert the matching pattern in the reactant SMARTS to a specified pattern in the product SMARTS (e.g., using RDKit [29]), and the synthetic pathway  $\mathbf{p}$  is defined as a specific ordering of these reaction steps. Given the target molecule  $\mathbf{x}$  as input, the goal of synthesizable projection is to generate the pathway  $\mathbf{p}$  that produces the end product molecule that is similar to  $\mathbf{x}$ :

$$\mathbf{p}^* = \underset{\mathbf{p}}{\operatorname{argmax}} \operatorname{sim}(\operatorname{prod}(\mathbf{p}), \mathbf{x}), \quad (1)$$

where  $\operatorname{sim} \in [0, 1]$  is the pairwise molecular similarity and  $\operatorname{prod}$  is the function that gets the end product by executing the pathway.

**Postfix notation of synthesis.** Prior works [36, 16] represent a synthetic pathway  $\mathbf{p}$  using a post-order traversal of its corresponding synthetic tree (Figure 2(a)). This representation captures synthesis as a bi-level sequence consists of the token type level and the token feature level. At the token type level, each token is one of four types: [START], [BB] (building block), [RXN] (reaction), or [END]. At the token feature level, different embedding strategies are used based on the token types: [BB] tokens are embedded using Morgan fingerprints since the set of purchasable building blocks is large and depends on purchasable stock catalogs, while [RXN] and other fixed tokens use the standard lookup embeddings. To match this bi-level representation, inference is performed hierarchically: a classifier first predicts the token type, then depending on the outcome, either a fingerprint network predicts the building block or a classifier selects the reaction. This representation can describe both linear and convergent synthetic pathways, and has been shown effective in bottom-up synthesis planning [36, 16], especially due to its compatibility with autoregressive generation.

#### 3.2. Representing Synthetic Pathways with Chain-of-Reaction Notation

Although the postfix notation is a simple and expressive method for representing synthetic pathways, it has several limitations that hinder generalized and effective pathway generation. First, given the final product molecule, the model needs to predict the entire synthetic pathway consisting of multiple reaction steps, solely by implicitly learning the reaction rule. Secondly, because the model must perform bi-level hierarchical prediction, it is prone to error accumulation, requiring additional architectural complexity. For example, Luo et al. [36] uses separate classifier heads for token type, reaction, and building block fingerprints, and Gao et al. [16] uses an additional Bernoulli diffusion head for building block fingerprints. In addition, the postfix notation uses Morgan fingerprints as the representation for building blocks. Since the mapping between a molecule and its fingerprints is not bijective, there exists information loss in both the embedding and prediction of building blocks. Furthermore, molecular fingerprints do not provide structurally smooth representation of molecules and a mistake in a single entry in the fingerprints can result in a significantly different molecule, making them not well-suited to representing reactants in synthetic reactions.

To overcome these limitations while maintaining the advantages of the postfix notation, we propose the *chain-of-reaction (CoR) notation* of synthesis (Figure 2(b)). While the CoR notation does not lose generality for synthetic pathways (i.e., can consider any synthetic pathways, whether linear or convergent), it has three important differences from the postfix notation: it (1) incorporates CoT at the chemical reaction level, (2) allows full pathway prediction without hierarchical classification, and (3) removes the dependence on molecular fingerprints.

To incorporate CoT in the design of synthesizable molecules and their synthetic pathways, we propose injecting the information of intermediate molecules along the pathways in  $\mathbf{p}$  (Figure 1). Under autoregressive modeling, the intermediates can be easily computed by executing the reaction after the reactant and reaction tokens are generated. By inserting intermediate molecules after each reaction to augment the pathway sequence, the model can explicitly learn reaction rules during training. Specifically, a pathway sequence  $\mathbf{p}$  in the CoR notation consists of  $B$  blocks (i.e., subsequences), where each block  $b \in \{1, \dots, B\}$  represents either a reaction, a molecule, the start or end of the sequence, all under a single unified token vocabulary:

$$\mathbf{p} := \mathbf{p}^1 \oplus \mathbf{p}^2 \oplus \dots \oplus \mathbf{p}^B, \quad (2)$$

where  $\oplus$  denotes the concatenation operation and  $\mathbf{p}^b$  denotes the  $b$ -th block of  $\mathbf{p}$ . Molecular blocks are represented by the Simplified Molecular Input Line Entry System (SMILES) [54] with additional tokens indicating the start and end of the block, while other types of blocks consist of a single token. Here, a molecular block can be either a building block or an intermediate. This representation also allows the model to encode and generate molecules without loss of information using SMILES, which is a smoother representation than molecular fingerprints for reactants and products in terms of molecular structure and reaction compatibility. Examples are provided in Section C.1.

### 3.3. Learning Chain-of-Reaction with Two Stages

**Supervised learning.** Inspired by SFT and RL finetuning for CoT reasoning in the LLM domain, we adopt a two-stage training scheme to learn the CoR notation. In the supervised learning stage, the Transformer  $\pi_\theta$  is trained on a dataset  $\mathcal{D}_{\text{SL}}$  of (question, CoT) pairs, i.e.,  $(\mathbf{x}, \mathbf{p})$ , with the next token prediction loss. Given  $\mathbf{x}$  encoded by the Transformer encoder, the Transformer decoder aims to autoregressively generate  $\mathbf{p}$ . Importantly, since molecular blocks comprise multiple SMILES tokens while other blocks comprise a single token, we introduce a loss weighting scheme based on token type:

$$\mathcal{L}_{\text{SL}} = - \mathbb{E}_{(\mathbf{x}, \mathbf{p}) \sim \mathcal{D}_{\text{SL}}} \left[ \frac{1}{|\mathcal{I}_{\text{SMILES}}|} \sum_{i \in \mathcal{I}_{\text{SMILES}}} \log \pi_\theta(\mathbf{p}_i | \mathbf{x}, \mathbf{p}_{1:i-1}) + \frac{1}{|\mathcal{I}_{\text{other}}|} \sum_{j \in \mathcal{I}_{\text{other}}} \log \pi_\theta(\mathbf{p}_j | \mathbf{x}, \mathbf{p}_{1:j-1}) \right], \quad (3)$$

where  $\mathcal{I}_{\text{SMILES}}$  and  $\mathcal{I}_{\text{other}}$  are the sets of SMILES token indices and non-SMILES token indices, respectively, and  $\mathbf{p}_i$  denotes the  $i$ -th token of  $\mathbf{p}$ . This balances the learning of synthesis pathways regardless of the type and number of reactions, building blocks, or intermediates in them. Note that intermediate tokens in the CoR notation directly allow the model to receive denser training signals in supervised learning. Further details are included in Section D.1.

**RL finetuning.** While the model can learn to generate synthetic pathways that project given molecules into the synthesizable chemical space with supervised learning, there can be multiple pathways that lead to the same product molecule. Inspired by Trung et al. [49], we propose to further improve the model’s reasoning ability through sampling various synthetic pathways. In this stage, the model  $\pi_\theta$  is trained on a dataset  $\mathcal{D}_{\text{RL}}$  composed of  $\mathbf{x}$  using an online RL algorithm:

$$\mathcal{L}_{\text{RL}} = \mathbb{E}_{\mathbf{x} \sim \mathcal{D}_{\text{RL}}, \mathbf{p} \sim \pi_\theta(\mathbf{p} | \mathbf{x})} [-r(\mathbf{p}, \mathbf{x})] + \beta \mathbb{D}_{\text{KL}}[\pi_\theta || \pi_{\text{ref}}], \quad (4)$$

where  $r$  is the reward function and the Kullback-Leibler (KL) divergence [28] term  $\mathbb{D}_{\text{KL}}$  is to prevent the model from deviating too far from the initial model.  $\pi_{\text{ref}}$  is the model trained with supervised learning which is also used for initializing  $\pi_\theta$  at the beginning of the RL finetuning stage and  $\beta$  is the coefficient of the divergence term. We employ Group Relative Policy Optimization (GRPO) [43], a variant of Proximal Policy Optimization (PPO) [41], with outcome supervision to optimize Eq. (4). The reward of a pathway  $\mathbf{p}$  given a target molecule  $\mathbf{x}$  is set to the molecular similarity between the generated product molecule  $\text{prod}(\mathbf{p})$  and

$\mathbf{x}$ , i.e.,  $r(\mathbf{p}, \mathbf{x}) = \text{sim}(\text{prod}(\mathbf{p}), \mathbf{x})$ . Note that the reward is only applied to the final outcome of the generation (i.e.,  $\text{prod}(\mathbf{p})$ ) and is independent of the reasoning path (i.e.,  $\mathbf{p}$ ), in contrast to the supervised learning stage which supervises the entire pathway. Through this stage, the model is endowed with the ability to explore diverse synthetic pathways with richer learning signals. Considering a pathway as an executable program that outputs a product molecule, this approach can be also viewed as analogous to leveraging code execution feedback in RL finetuning of code generation LLMs [30, 32]. Further details are included in Section D.2.

### 3.4. Inference with Test-time Compute Scaling

During inference, a stack is maintained for each pathway that is being generated, following Luo et al. [36] and Gao et al. [16]. If the model predicts a [BB] block in SMILES, the nearest building block is retrieved from the building block set and pushed to the stack. If the model predicts a [RXN] block, the required number of reactants are popped from the top of the stack to execute the reaction, and the obtained intermediate molecule is pushed back to the stack. Importantly, the intermediate is added not only to the stack but also to the sequence being generated by the decoder, providing richer information about the pathway and allowing step-by-step reasoning.

Following previous works [36, 16], we employ beam search which tracks the top-scoring stacks and expands them block-by-block. Here, we introduce a different scoring function for each task. In synthesizable molecule reconstruction (Section 4.1) where the objective is to reconstruct input molecules by proposing their synthetic pathways, [BB] blocks are scored by the similarity to the generated SMILES, which was used in the building block retrieval step. [RXN] blocks are scored by the classification probability predicted by the model, and a stack’s score is defined as the sum of the scores of its blocks.

On the other hand, for synthesizable goal-directed molecular optimization (Section 4.2) or synthesizable hit expansion (Section 4.3), we use ReaSyn to project optimized models or generated hits. The objective is not only to generate synthesizable analogs to the input molecule, but also to suggest synthesizable molecules with high target chemical properties. Therefore, we propose to guide the search using a reward model that predicts the optimization objective. For example, a neural network trained to predict the target chemical property or an external scoring function can be used as the reward model. Using the reward model, [BB] blocks are scored by the predicted property of the building block and [RXN] blocks are scored by the predicted property of the intermediate product obtained by executing the pathway generated so far. This search mechanism using the reward model allows us to leverage test-time compute scaling scheme [45] tailored for goal-directed synthesizable projection, guiding the exploration in the synthesizable space with desired chemical properties.

## 4. Experiments

Following Gao et al. [16], we adopt the set of 115 reactions that include common uni-, bi- and tri-molecular reactions, and the set of 211,220 purchasable building blocks in the Enamine’s U.S. stock catalog retrieved in October 2023 [10], together covering a synthesizable chemical space broader than  $10^{60}$  molecules. The details regarding the Transformer architecture are included in Section C.2.

### 4.1. Synthesizable Molecule Reconstruction

**Setup.** Even given a vast synthesizable space, previous synthesizable molecule generation methods have struggled to cover this space extensively. We evaluate the coverage of ReaSyn in the synthesizable chemical space with synthesizable molecule reconstruction, where the goal is to reconstruct given molecules by proposing synthetic pathways. Following Gao et al. [16], the reconstruction is evaluated on randomly selected 1,000 molecules from the Enamine REAL diversity set [10] and ChEMBL [17]. In addition, to simulate common real-world scenarios in which the set of purchasable building blocks expands after the model is trained, we include another challenging benchmark by expanding the building block set with unseen building blocks. Concretely, we add 37,386 molecules with fewer than 18 heavy atoms from ZINC250k [23], yielding a total of 248,606 building blocks. 1,000 molecules generated using the defined reaction rules and the new building blocks are used as the test set. We also experiment with another test set of ChEMBL molecules introduced by Luo et al. [36]. Further details are included in Section E.1.

**Metrics.** Following Gao et al. [16], **reconstruction rate**, the fraction of generated pathways that yield the identical product molecule to the input molecule, and **similarity**, the average Tanimoto similarity on

Table 1 | **Synthesizable molecule reconstruction results.** The results are the means and the standard deviations of 3 runs. The best results are highlighted in bold.

Dataset	Method	Reconstruction rate (%)	Similarity	Div. (Pathway)	Div. (BB)
Enamine	SynNet [14]	25.2 $\pm$ 0.1	0.661 $\pm$ 0.000	0.014 $\pm$ 0.001	0.239 $\pm$ 0.002
	SynFormer [16]	63.5 $\pm$ 0.9	0.900 $\pm$ 0.001	0.104 $\pm$ 0.001	0.554 $\pm$ 0.003
	ReaSyn (ours)	<b>76.8</b> $\pm$ 0.7	<b>0.946</b> $\pm$ 0.002	<b>0.148</b> $\pm$ 0.002	<b>0.638</b> $\pm$ 0.003
ChEMBL	SynNet [14]	7.9 $\pm$ 0.0	0.542 $\pm$ 0.000	0.009 $\pm$ 0.000	0.090 $\pm$ 0.001
	SynFormer [16]	18.2 $\pm$ 0.7	0.645 $\pm$ 0.002	0.038 $\pm$ 0.001	0.187 $\pm$ 0.002
	ReaSyn (ours)	<b>21.9</b> $\pm$ 0.2	<b>0.676</b> $\pm$ 0.000	<b>0.049</b> $\pm$ 0.002	<b>0.226</b> $\pm$ 0.003
ZINC250k	SynNet [14]	12.6 $\pm$ 0.1	0.456 $\pm$ 0.001	0.001 $\pm$ 0.000	0.089 $\pm$ 0.000
	SynFormer [16]	15.1 $\pm$ 1.5	0.525 $\pm$ 0.004	0.017 $\pm$ 0.000	0.136 $\pm$ 0.001
	ReaSyn (ours)	<b>41.2</b> $\pm$ 0.2	<b>0.735</b> $\pm$ 0.001	<b>0.070</b> $\pm$ 0.001	<b>0.361</b> $\pm$ 0.002

Table 2 | **Synthesizable molecule reconstruction results** with the ChEMBL test set in Luo et al. [36]. The results of SynNet [14] and ChemProjector [36] are taken from Luo et al. [36].

Method	Reconstruction rate (%)	Sim. (Morgan)	Sim. (Scaffold)	Sim. (Gobbi)
SynNet [14]	5.4	0.427	0.417	0.268
ChemProjector [36]	13.4	0.616	0.603	0.564
SynFormer [16]	19.1 $\pm$ 0.2	0.668 $\pm$ 0.002	0.640 $\pm$ 0.004	0.615 $\pm$ 0.004
ReaSyn (ours)	<b>22.9</b> $\pm$ 0.3	<b>0.693</b> $\pm$ 0.002	<b>0.673</b> $\pm$ 0.001	<b>0.635</b> $\pm$ 0.001

the Morgan fingerprint [37] between the generated molecule and the input molecule, are used to evaluate the model. We further report **diversity (pathway)**, the average molecular diversity of end products from analogous pathways, and **diversity (BB)**, the average diversity of unique building blocks in analogous pathways, to assess diversity of generation. Here, *analogous pathways* are defined as pathways that yield a product molecule with a Tanimoto similarity  $\geq 0.8$  to the input molecule. For the experiment with the test set of Luo et al. [36], **similarity** between the input target molecule and the projected analog is measured using the Tanimoto similarity on three molecular fingerprints: (1) Morgan fingerprint [37], (2) Morgan fingerprint of Murcko scaffold, and (3) Gobbi pharmacophore fingerprint [19], following Luo et al. [36].

**Results.** In Table 1 and Table 2, we compare ReaSyn with state-of-the-art synthesizable analog generation methods, SynNet [14] and SynFormer [16]. ReaSyn significantly outperforms the baselines across all metrics. Specifically, ReaSyn shows a high reconstruction rate and similarity, demonstrating that it successfully reconstructs input molecules by extensively exploring a synthesizable chemical space. In Table 1, it also shows high diversity, demonstrating its ability to propose diverse pathways. Note that unlike the Enamine and ZINC250k test sets, molecules in the ChEMBL test set may lie beyond the defined synthesizable space (i.e., may require reactions or building blocks that are not given), so the model performance is generally low on ChEMBL. Notably, ReaSyn outperforms the baselines by a particularly large margin on the ZINC250k test set, which simulates challenging scenarios with out-of-distribution test molecules and unseen building blocks. This result highlights the strong generalizability and robustness of ReaSyn in generating out-of-distribution synthetic pathways.

#### 4.2. Synthesizable Goal-directed Molecular Optimization

While goal-directed molecular optimization methods aim to address essential drug discovery tasks, their practicality is limited as the generated molecules are often not synthesizable [13]. To overcome this problem, synthesizable projection can be applied to goal-directed molecular optimization. Similar to Gao et al. [16], we demonstrate the application of ReaSyn in exploring the local synthesizable space in conjunction with an off-the-shelf molecular optimization method. Specifically, we use synthesizable projection of ReaSyn as an additional mutation operator of a genetic algorithm (GA) by projecting the offspring molecules after every reproduction step of Graph GA [24], thus ensuring all the resulting offspring molecules lie in the synthesizable space. We denote the resulting GA as Graph GA-ReaSyn. We emphasize that this approach is universal and other molecular optimization methods can also be used. A property predictor is trained on-the-fly during the optimization process to predict the target property and set as the reward model to guide the search. Further details are included in Section E.2.

Table 3 | **Synthesizable goal-directed molecular optimization results on the TDC oracles.** The results are the means of AUC top-10 and average top-10 SA scores of 3 runs. The results for the baselines other than Graph GA-SF and Graph GA are taken from Sun et al. [46]. The best synthesis-based results are highlighted in bold.

Method Synthesis	Graph GA-ReaSyn ✓	Graph GA-SF [16] ✓	SynthesisNet [46] ✓	SynNet [14] ✓	DoG-Gen [3] ✓	DoG-AE [3] ✓	Graph GA [24] ✗
amlodipine_mpo	0.678	<b>0.696</b>	0.608	0.567	0.537	0.509	0.651
celecoxib_rediscovery	<b>0.754</b>	0.559	0.582	0.443	0.466	0.357	0.682
drd2	<b>0.973</b>	0.972	0.960	0.969	0.949	0.944	0.970
feoxefenadine_mpo	0.788	0.786	<b>0.791</b>	0.764	0.697	0.681	0.785
gsk3b	<b>0.851</b>	0.803	0.848	0.790	0.832	0.602	0.838
jnk3	<b>0.741</b>	0.658	0.639	0.631	0.596	0.470	0.693
median1	0.293	<b>0.308</b>	0.305	0.219	0.218	0.172	0.261
median2	<b>0.259</b>	0.258	0.257	0.237	0.213	0.183	0.257
osimertinib_mpo	<b>0.820</b>	0.816	0.810	0.797	0.776	0.751	0.829
perindopril_mpo	0.560	0.530	0.524	0.559	0.475	0.433	0.533
ranolazine_mpo	0.742	<b>0.751</b>	0.741	0.743	0.712	0.690	0.745
sitagliptin_mpo	<b>0.342</b>	0.338	0.313	0.026	0.048	0.010	0.524
zaleplon_mpo	0.492	0.478	<b>0.528</b>	0.341	0.123	0.050	0.458
Average score	<b>0.638</b>	0.612	0.608	0.545	0.511	0.450	0.633
SA score ↓	2.953	2.995	<b>2.739</b>	3.071	2.793	2.857	3.494

Table 4 | **Synthesizable goal-directed molecular optimization results on the sEH proxy.** The results are the means and the standard deviations of 3 runs. The results for the baselines are taken from Cretu et al. [7]. The best results are highlighted in bold.

Method	Synthesis	sEH	SA ↓	QED
FragGFN [1]	✗	0.77 ± 0.01	6.28 ± 0.02	0.30 ± 0.01
FragGFN (SA) [1]	✗	0.70 ± 0.01	5.45 ± 0.05	0.29 ± 0.01
SyntheMol [47]	✓	0.64 ± 0.01	3.08 ± 0.01	0.63 ± 0.01
SynFlowNet [7]	✓	0.92 ± 0.01	2.92 ± 0.01	0.59 ± 0.02
SynFlowNet (SA) [7]	✓	0.94 ± 0.01	2.67 ± 0.03	0.68 ± 0.01
SynFlowNet (QED) [7]	✓	0.86 ± 0.03	4.02 ± 0.26	0.74 ± 0.04
Graph GA-ReaSyn (ours)	✓	<b>0.97</b> ± 0.01	<b>2.01</b> ± 0.02	<b>0.75</b> ± 0.01

Table 5 | **JNK3 hit expansion results.** The results are the means and the standard deviations of 3 runs. The best results are highlighted in bold.

Method	Analog rate (%)	Improve rate (%)	Success rate (%)
SynNet [14]	15.1 ± 0.1	1.5 ± 0.0	1.3 ± 0.0
SynFormer [16]	38.9 ± 2.7	7.1 ± 0.4	5.4 ± 0.3
ReaSyn (ours)	<b>50.0</b> ± 1.2	<b>13.1</b> ± 0.3	<b>11.3</b> ± 0.8

#### 4.2.1. Optimization of TDC Oracles

**Setup.** Following Sun et al. [46], we conduct 15 goal-directed molecular optimization tasks of the benchmark of Gao et al. [15] that simulate real-world drug discovery with the TDC oracle functions [22], and use the **AUC top-10** to assess the optimization performance. We also report **synthetic accessibility (SA) score** [11] of the top-10 optimized molecules to cross-validate the synthesizability.

**Results.** The results are shown in Table 3. We compare Graph GA-ReaSyn with synthesis-based baselines that restrict the generation to the synthesizable chemical space. We also include Graph GA [24] to examine the impact of the synthesizable projection. Graph GA-ReaSyn outperforms all synthesis-based baselines in optimization performance, showing its effectiveness in discovering chemical optima in the synthesizable space. Notably, it achieves comparable optimization performance to Graph GA with much superior SA score, validating that the proposed synthesizable projection can generate synthesizable analogs while maintaining the core molecular properties.

#### 4.2.2. Optimization of sEH Binding Affinity

**Setup.** Following Cretu et al. [7], we conduct optimization of the binding affinity against the protein target soluble epoxide hydrolase (sEH), measured by a pretrained proxy model [1]. As the evaluation metrics, the average **binding affinity**, **SA score**, and quantitative estimate of drug-likeness (**QED**) [2] of generated molecules are reported.

**Results.** The results are shown in Table 4. FragGFN [1] and SynFlowNet [7] are GFlowNets [1] with a fragment action space and a reaction action space, respectively, and SyntheMol [47] is a property predictor-guided MCTS method. ‘(SA)’ or ‘(QED)’ denote using a modified optimization objective with SA score or QED. All baselines except FragGFN take the approach of constraining the design space to the synthesizable space. As shown in the table, ReaSyn outperforms previous methods in terms of sEH binding affinity, SA score,

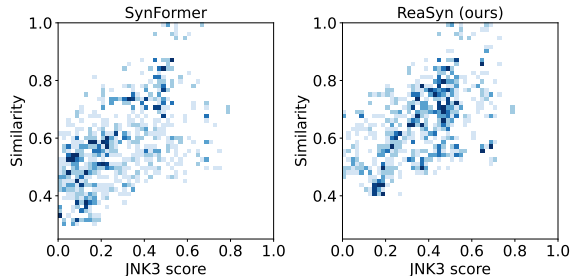


Figure 3 | The distribution of JNK3 scores and analog similarity of SynFormer and ReaSyn.

Table 6 | Ablation study on synthesizable analog generation. The best results are highlighted in bold.

Dataset	Method	Rec. rate (%)	Similarity	Div. (Pathway)	Div. (BB)
Enamine	ReaSyn	<b>76.8</b>	<b>0.946</b>	<b>0.148</b>	<b>0.638</b>
	- RL	76.1	0.944	0.146	0.636
	- INT	74.7	0.940	0.126	0.636
ChEMBL	ReaSyn	<b>21.9</b>	<b>0.676</b>	<b>0.049</b>	<b>0.226</b>
	- RL	21.6	0.674	<b>0.049</b>	0.225
	- INT	21.5	0.672	0.045	0.209
ZINC250k	ReaSyn	41.2	0.735	<b>0.070</b>	<b>0.361</b>
	- RL	40.4	0.733	0.068	<b>0.361</b>
	- INT	<b>43.8</b>	<b>0.748</b>	0.063	0.356

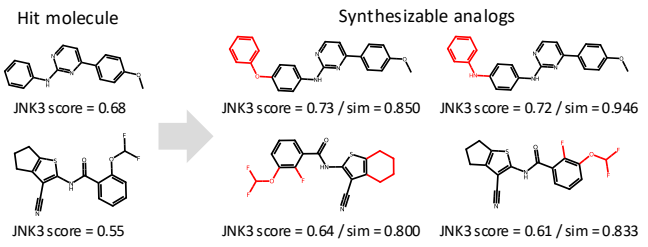


Figure 4 | Examples of generated synthesizable analogs from JNK3 hit expansion. Modified substructures in the analogs are indicated by red.

Table 7 | Ablation study on synthesizable goal-directed molecular optimization with the TDC oracles.

Method	Average score	SA score ↓
Graph GA-ReaSyn	<b>0.638</b>	<b>2.953</b>
- Goal reward	0.619	2.955

Table 8 | Ablation study on synthesizable hit expansion.

Method	Analog rate (%)	Improve rate (%)	Success rate (%)
ReaSyn	50.0	<b>13.1</b>	<b>11.3</b>
- Goal reward	<b>62.6</b>	12.5	7.0

and QED, verifying that synthesizable projection using ReaSyn is a more effective strategy to find synthesizable chemical optima. Note that FragGPN shows a very poor SA score because it does not consider synthesizability.

#### 4.3. Synthesizable Hit Expansion

**Setup.** Synthesizable projection of ReaSyn can suggest multiple synthesizable analogs for a given target molecule with a beam search, and thus can be applied to hit expansion to find synthesizable analogs of hit molecules. Following Gao et al. [16], we conduct hit expansion on the identified hit molecules for c-Jun NH2-terminal kinase 3 (JNK3) inhibition. Specifically, the proxy from the TDC library [22] is used as the oracle function that scores the inhibition of JNK3, and the top-10 scoring molecule from ZINC250k [23] are selected as the hits. The JNK3 proxy is set as the reward model to guide the search and 100 analogs are generated for each hit, yielding a total of 1,000 synthesizable molecules. **Analog rate**, the fraction of generated analogs that have Tanimoto similarities  $\geq 0.6$  to the input hit, **improve rate**, the fraction of generated analogs that have higher JNK3 scores than the original hit, and **success rate**, the fraction of generated analogs that satisfy both, are computed by averaging over the generated molecules. Further details are included in Section E.3.

**Results.** The results are shown in Table 5. ReaSyn exhibits superior performance to the previous synthesizable projection methods in terms of all metrics. The high analog rate shows that ReaSyn can broadly search the synthesizable space to suggest close analogs thanks to the CoR notation, while the high improve rate shows that ReaSyn can find chemical optima in terms of the target property thanks to the goal-directed search. We also provide the distribution of suggested molecules in Figure 3 and examples in Figure 4. Compared to SynFormer, ReaSyn generates synthesizable molecules with high similarities and high JNK3 inhibition scores, highlighting its effectiveness in hit expansion.

#### 4.4. Ablation Study

**CoR notation and RL finetuning.** To examine the effect of the intermediate product token blocks in the CoR notation and RL finetuning, we conduct ablation studies in Table 6. ReaSyn without RL finetuning shows degraded the performance on most metrics. In addition, removing the intermediate product token token blocks in the

CoR notation further degraded the performance and diversity, demonstrating that the intermediate product token blocks are important for suggesting diverse synthetic pathways that yield a given molecule. While both factors contribute to the performance of ReaSyn, we observe that the usage of the intermediate token blocks has more significant impact on generating synthesizable analogs. These results indicate that the explorability of ReaSyn in the synthesizable chemical space largely stems from the step-by-step reasoning with the CoR notation. On the other hand, to verify the superiority of SMILES over molecular fingerprints, we implemented a model that uses fingerprints instead of SMILES in the CoR notation. However, we observed that the concatenation of fingerprints resulted in (1) very long sequences and (2) severe token imbalance under a unified token vocabulary since the fingerprints are very sparse, preventing the model from being properly trained.

**Goal-directed search with the reward model.** To analyze the effect of the proposed search strategy with the reward model in synthesizable goal-directed molecular optimization, we present the results of ReaSyn without it in Table 7 and Table 8. Instead of training a goal-directed reward model on-the-fly, the ablated ReaSyn employs the similarity between the target and intermediates as the scoring function in the search during inference, as in synthesizable molecule reconstruction. ReaSyn without the goal-directed reward search shows degraded performance in most metrics, verifying the importance of the goal-directed guidance using the reward model. Because it uses similarity to guide the search, it naturally exhibits a higher analog rate in the JNK3 hit expansion task, but this is at the expense of optimization performance and results in a lower success rate overall.

## 5. Conclusion

A major weakness of molecular generative models is the generation of synthetically inaccessible molecules. In our paper, we introduced ReaSyn, an effective framework for synthesizable projection that frames synthetic pathways as CoT reasoning paths using the CoR notation. By explicitly including reactants, reaction types, and intermediate products at each step, the CoR notation allows ReaSyn to have the step-by-step reasoning capability. We further proposed to enhance the reasoning ability of ReaSyn via RL finetuning and goal-directed test-time compute scaling. We experimentally validated that ReaSyn exhibits significantly improved exploration in the synthesizable chemical space with high molecular reconstruction rates, pathway diversity, optimization scores, and hit expansion performance, showing its potential as a practical tool for real-world drug discovery.

## References

- [1] Emmanuel Bengio, Moksh Jain, Maksym Korablyov, Doina Precup, and Yoshua Bengio. Flow network based generative models for non-iterative diverse candidate generation. *Advances in Neural Information Processing Systems*, 34:27381–27394, 2021.
- [2] G Richard Bickerton, Gaia V Paolini, Jérémie Besnard, Sorel Muresan, and Andrew L Hopkins. Quantifying the chemical beauty of drugs. *Nature chemistry*, 4(2):90–98, 2012.
- [3] John Bradshaw, Brooks Paige, Matt J Kusner, Marwin Segler, and José Miguel Hernández-Lobato. Barking up the right tree: an approach to search over molecule synthesis dags. *Advances in neural information processing systems*, 33:6852–6866, 2020.
- [4] Karl Cobbe, Vineet Kosaraju, Mohammad Bavarian, Mark Chen, Heewoo Jun, Lukasz Kaiser, Matthias Plappert, Jerry Tworek, Jacob Hilton, Reiichiro Nakano, et al. Training verifiers to solve math word problems. *arXiv preprint arXiv:2110.14168*, 2021.
- [5] Connor W Coley, Luke Rogers, William H Green, and Klavs F Jensen. Scscore: synthetic complexity learned from a reaction corpus. *Journal of chemical information and modeling*, 58(2):252–261, 2018.
- [6] Connor W Coley, Dale A Thomas III, Justin AM Lummiss, Jonathan N Jaworski, Christopher P Breen, Victor Schultz, Travis Hart, Joshua S Fishman, Luke Rogers, Hanyu Gao, et al. A robotic platform for flow synthesis of organic compounds informed by ai planning. *Science*, 365(6453):eaax1566, 2019.
- [7] Miruna Cretu, Charles Harris, Julien Roy, Emmanuel Bengio, and Pietro Liò. Synflownet: Towards molecule design with guaranteed synthesis pathways. In *International Conference on Learning Representations*, 2025.

- [8] Inc. Daylight Chemical Information Systems. Smarts-a language for describing molecular patterns, 2019. URL <https://www.daylight.com/dayhtml/doc/theory/theory.smarts.html>.
- [9] Hanze Dong, Wei Xiong, Deepanshu Goyal, Yihan Zhang, Winnie Chow, Rui Pan, Shizhe Diao, Jipeng Zhang, Kashun Shum, and Tong Zhang. Raft: Reward ranked finetuning for generative foundation model alignment. *Transactions on Machine Learning Research*, 2023.
- [10] Enamine. Building blocks catalog, 2023. URL <https://enamine.net/building-blocks/building-blocks-catalog>.
- [11] Peter Ertl and Ansgar Schuffenhauer. Estimation of synthetic accessibility score of drug-like molecules based on molecular complexity and fragment contributions. *Journal of cheminformatics*, 1:1–11, 2009.
- [12] Xidong Feng, Ziyu Wan, Muning Wen, Stephen Marcus McAleer, Ying Wen, Weinan Zhang, and Jun Wang. Alphazero-like tree-search can guide large language model decoding and training. *arXiv preprint arXiv:2309.17179*, 2023.
- [13] Wenhao Gao and Connor W Coley. The synthesizability of molecules proposed by generative models. *Journal of chemical information and modeling*, 60(12):5714–5723, 2020.
- [14] Wenhao Gao, Rocío Mercado, and Connor W Coley. Amortized tree generation for bottom-up synthesis planning and synthesizable molecular design. In *International Conference on Learning Representations*, 2021.
- [15] Wenhao Gao, Tianfan Fu, Jimeng Sun, and Connor Coley. Sample efficiency matters: a benchmark for practical molecular optimization. *Advances in Neural Information Processing Systems*, 35:21342–21357, 2022.
- [16] Wenhao Gao, Shitong Luo, and Connor W Coley. Generative artificial intelligence for navigating synthesizable chemical space. *arXiv preprint arXiv:2410.03494*, 2024.
- [17] Anna Gaulton, Louisa J Bellis, A Patricia Bento, Jon Chambers, Mark Davies, Anne Hersey, Yvonne Light, Shaun McGlinchey, David Michalovich, Bissan Al-Lazikani, et al. Chemb: a large-scale bioactivity database for drug discovery. *Nucleic acids research*, 40(D1):D1100–D1107, 2012.
- [18] Samuel Genheden, Amol Thakkar, Veronika Chadimová, Jean-Louis Reymond, Ola Engkvist, and Esben Bjerrum. Aizynthfinder: a fast, robust and flexible open-source software for retrosynthetic planning. *Journal of cheminformatics*, 12(1):70, 2020.
- [19] Alberto Gobbi and Dieter Poppinger. Genetic optimization of combinatorial libraries. *Biotechnology and bioengineering*, 61(1):47–54, 1998.
- [20] Caglar Gulcehre, Tom Le Paine, Srivatsan Srinivasan, Ksenia Konyushkova, Lotte Weerts, Abhishek Sharma, Aditya Siddhant, Alex Ahern, Miaosen Wang, Chenjie Gu, et al. Reinforced self-training (rest) for language modeling. *arXiv preprint arXiv:2308.08998*, 2023.
- [21] Daya Guo, Dejian Yang, Haowei Zhang, Junxiao Song, Ruoyu Zhang, Runxin Xu, Qihao Zhu, Shirong Ma, Peiyi Wang, Xiao Bi, et al. Deepseek-r1: Incentivizing reasoning capability in llms via reinforcement learning. *arXiv preprint arXiv:2501.12948*, 2025.
- [22] Kexin Huang, Tianfan Fu, Wenhao Gao, Yue Zhao, Yusuf H Roohani, Jure Leskovec, Connor W Coley, Cao Xiao, Jimeng Sun, and Marinka Zitnik. Therapeutics data commons: Machine learning datasets and tasks for drug discovery and development. In *NeurIPS Track Datasets and Benchmarks*, 2021.
- [23] John J Irwin, Teague Sterling, Michael M Mysinger, Erin S Bolstad, and Ryan G Coleman. Zinc: a free tool to discover chemistry for biology. *Journal of chemical information and modeling*, 52(7):1757–1768, 2012.
- [24] Jan H Jensen. A graph-based genetic algorithm and generative model/monte carlo tree search for the exploration of chemical space. *Chemical science*, 10(12):3567–3572, 2019.

[25] T Kim, S Lee, Y Kwak, MS Choi, J Park, SJ Hwang, and SG Kim. Readretro: natural product biosynthesis predicting with retrieval-augmented dual-view retrosynthesis. *The New Phytologist*, 2024.

[26] Ksenia Korovina, Sailun Xu, Kirthevasan Kandasamy, Willie Neiswanger, Barnabas Poczos, Jeff Schneider, and Eric Xing. Chembo: Bayesian optimization of small organic molecules with synthesizable recommendations. In *International Conference on Artificial Intelligence and Statistics*, pages 3393–3403. PMLR, 2020.

[27] Michał Koziarski, Andrei Rekesh, Dmytro Shevchuk, Almer van der Sloot, Piotr Gaiński, Yoshua Bengio, Chenghao Liu, Mike Tyers, and Robert Batey. Rgfn: Synthesizable molecular generation using gflownets. *Advances in Neural Information Processing Systems*, 37:46908–46955, 2024.

[28] Solomon Kullback and Richard A Leibler. On information and sufficiency. *The annals of mathematical statistics*, 22(1):79–86, 1951.

[29] Greg Landrum et al. RDKit: Open-source cheminformatics software, 2016. URL <http://www.rdkit.org/>, <https://github.com/rdkit/rdkit>.

[30] Hung Le, Yue Wang, Akhilesh Deepak Gotmare, Silvio Savarese, and Steven Chu Hong Hoi. Coderl: Mastering code generation through pretrained models and deep reinforcement learning. *Advances in Neural Information Processing Systems*, 35:21314–21328, 2022.

[31] Hunter Lightman, Vineet Kosaraju, Yuri Burda, Harrison Edwards, Bowen Baker, Teddy Lee, Jan Leike, John Schulman, Ilya Sutskever, and Karl Cobbe. Let’s verify step by step. In *International Conference on Learning Representations*, 2024.

[32] Jiate Liu, Yiqin Zhu, Kaiwen Xiao, QIANG FU, Xiao Han, Yang Wei, and Deheng Ye. Rlrf: Reinforcement learning from unit test feedback. *Transactions on Machine Learning Research*, 2023.

[33] Ilya Loshchilov and Frank Hutter. Decoupled weight decay regularization. *International Conference on Learning Representations*, 2019.

[34] Daniel Lowe. Chemical reactions from us patents, 2017. URL [https://figshare.com/articles/dataset/Chemical\\_reactions\\_from\\_US\\_patents\\_1976-Sep2016\\_/5104873](https://figshare.com/articles/dataset/Chemical_reactions_from_US_patents_1976-Sep2016_/5104873).

[35] Haipeng Luo, Qingfeng Sun, Can Xu, Pu Zhao, Jianguang Lou, Chongyang Tao, Xiubo Geng, Qingwei Lin, Shifeng Chen, and Dongmei Zhang. Wizardmath: Empowering mathematical reasoning for large language models via reinforced evol-instruct. *arXiv preprint arXiv:2308.09583*, 2023.

[36] Shitong Luo, Wenhao Gao, Zuofan Wu, Jian Peng, Connor W Coley, and Jianzhu Ma. Projecting molecules into synthesizable chemical spaces. In *International Conference on Machine Learning*, pages 33289–33304. PMLR, 2024.

[37] Harry L Morgan. The generation of a unique machine description for chemical structures-a technique developed at chemical abstracts service. *Journal of chemical documentation*, 5(2):107–113, 1965.

[38] OpenAI. Introducing deep research, 2025. URL <https://openai.com/index/introducing-deep-research>.

[39] Aryan Pedawi, Paweł Gniewek, Chaoyi Chang, Brandon Anderson, and Henry van den Bedem. An efficient graph generative model for navigating ultra-large combinatorial synthesis libraries. *Advances in Neural Information Processing Systems*, 35:8731–8745, 2022.

[40] Rafael Rafailev, Archit Sharma, Eric Mitchell, Christopher D Manning, Stefano Ermon, and Chelsea Finn. Direct preference optimization: Your language model is secretly a reward model. *Advances in Neural Information Processing Systems*, 36:53728–53741, 2023.

[41] John Schulman, Filip Wolski, Prafulla Dhariwal, Alec Radford, and Oleg Klimov. Proximal policy optimization algorithms. *arXiv preprint arXiv:1707.06347*, 2017.

[42] Seonghwan Seo, Minsu Kim, Tony Shen, Martin Ester, Jinkyoo Park, Sungsoo Ahn, and Woo Youn Kim. Generative flows on synthetic pathway for drug design. *International Conference on Learning Representations*, 2025.

[43] Zhihong Shao, Peiyi Wang, Qihao Zhu, Runxin Xu, Junxiao Song, Xiao Bi, Haowei Zhang, Mingchuan Zhang, YK Li, Y Wu, et al. Deepseekmath: Pushing the limits of mathematical reasoning in open language models. *arXiv preprint arXiv:2402.03300*, 2024.

[44] Avi Singh, John D Co-Reyes, Rishabh Agarwal, Ankesh Anand, Piyush Patil, Xavier Garcia, Peter J Liu, James Harrison, Jaehoon Lee, Kelvin Xu, et al. Beyond human data: Scaling self-training for problem-solving with language models. *arXiv preprint arXiv:2312.06585*, 2023.

[45] Charlie Snell, Jaehoon Lee, Kelvin Xu, and Aviral Kumar. Scaling llm test-time compute optimally can be more effective than scaling model parameters. *arXiv preprint arXiv:2408.03314*, 2024.

[46] Michael Sun, Alston Lo, Minghao Guo, Jie Chen, Connor W Coley, and Wojciech Matusik. Procedural synthesis of synthesizable molecules. In *International Conference on Learning Representations*, 2025.

[47] Kyle Swanson, Gary Liu, Denise B Catacutan, Autumn Arnold, James Zou, and Jonathan M Stokes. Generative ai for designing and validating easily synthesizable and structurally novel antibiotics. *Nature Machine Intelligence*, 6(3):338–353, 2024.

[48] Amol Thakkar, Veronika Chadimová, Esben Jannik Bjerrum, Ola Engkvist, and Jean-Louis Reymond. Retrosynthetic accessibility score (rascore)—rapid machine learned synthesizability classification from ai driven retrosynthetic planning. *Chemical science*, 12(9):3339–3349, 2021.

[49] Luong Trung, Xinbo Zhang, Zhanming Jie, Peng Sun, Xiaoran Jin, and Hang Li. Reft: Reasoning with reinforced fine-tuning. In *Proceedings of the 62nd Annual Meeting of the Association for Computational Linguistics*, 2024.

[50] Ashish Vaswani, Noam Shazeer, Niki Parmar, Jakob Uszkoreit, Llion Jones, Aidan N Gomez, Łukasz Kaiser, and Illia Polosukhin. Attention is all you need. *Advances in neural information processing systems*, 30, 2017.

[51] W Patrick Walters and Regina Barzilay. Critical assessment of ai in drug discovery. *Expert opinion on drug discovery*, 16(9):937–947, 2021.

[52] Ke Wang, Houxing Ren, Aojun Zhou, Zimu Lu, Sichun Luo, Weikang Shi, Renrui Zhang, Linqi Song, Mingjie Zhan, and Hongsheng Li. Mathcoder: Seamless code integration in llms for enhanced mathematical reasoning. *arXiv preprint arXiv:2310.03731*, 2023.

[53] Jason Wei, Xuezhi Wang, Dale Schuurmans, Maarten Bosma, Fei Xia, Ed Chi, Quoc V Le, Denny Zhou, et al. Chain-of-thought prompting elicits reasoning in large language models. *Advances in neural information processing systems*, 35:24824–24837, 2022.

[54] David Weininger. Smiles, a chemical language and information system. 1. introduction to methodology and encoding rules. *Journal of chemical information and computer sciences*, 28(1):31–36, 1988.

[55] Shunyu Yao, Dian Yu, Jeffrey Zhao, Izhak Shafran, Tom Griffiths, Yuan Cao, and Karthik Narasimhan. Tree of thoughts: Deliberate problem solving with large language models. *Advances in neural information processing systems*, 36:11809–11822, 2023.

[56] Dan Zhang, Sining Zhoubian, Ziniu Hu, Yisong Yue, Yuxiao Dong, and Jie Tang. Rest-mcts\*: Llm self-training via process reward guided tree search. *Advances in Neural Information Processing Systems*, 37:64735–64772, 2024.

# Appendix

## A. Limitations

In this paper, we considered reactants, reaction rule, and products as the basic components that compose a chemical reaction, thus included this information in each reasoning step in the CoR notation. However, other information of reactions such as reagents or yields, can be important considerations in some drug discovery scenarios in real-world. These information can then be additionally incorporated into the reasoning step to enhance the reasoning capability of the model and improve its practical impact, and we left this as a future work.

## B. Broader Impacts

In our paper, we introduced ReaSyn and demonstrated its effectiveness as a practical tool for generating synthesizable drug candidates and accelerate real-world drug discovery pipelines. However, the proposed framework also has the possibility to generate synthetic pathways of toxic drugs. To prevent this, an additional scheme can be adopted to examine the toxicity of generated molecules or pathways and filters out harmful ones during the generation search.

## C. Details on Pathway Representation and Model

### C.1. CoR Notation

The CoR notation is parsed using a unified token vocabulary of size 272, including [START], [END], [MOL:START], [MOL:END], 153 SMILES tokens and 115 reaction tokens. The SMILES tokens include the following:

H, He, Li, Be, B, C, N, O, F, Ne, Na, Mg, Al, Si, P, S, Cl, Ar, K, Ca, Sc, Ti, V, Cr, Mn, Fe, Co, Ni, Cu, Zn, Ga, Ge, As, Se, Br, Kr, Rb, Sr, Y, Zr, Nb, Mo, Tc, Ru, Rh, Pd, Ag, Cd, In, Sn, Sb, Te, I, Xe, Cs, Ba, La, Ce, Pr, Nd, Pm, Sm, Eu, Gd, Tb, Dy, Ho, Er, Tm, Yb, Lu, Hf, Ta, W, Re, Os, Ir, Pt, Au, Hg, Tl, Pb, Bi, Po, At, Rn, Fr, Ra, Ac, Th, Pa, U, Np, Pu, Am, Cm, Bk, Cf, Es, Fm, Md, No, Lr, Rf, Db, Sg, Bh, Hs, Mt, Ds, Rg, Cn, Nh, Fl, Mc, Lv, Ts, Og, b, c, n, o, s, p, 0, 1, 2, 3, 4, 5, 6, 7, 8, 9, [ , ], ( , ), ., =, #, -, +, \, /, :, ~, @, ?, >, \*, \$, %

The input target molecules are also encoded using the above tokens.

We provide examples of *p* in the CoR notation. An example synthetic pathway of CN(CCNC(=O)CC1CCC2(CC1)CCC20)C(=O)c1cccc2ncnn12 (the middle one in Figure 6) is as follows:

```
[START] [MOL:START] O=C(O)c1cccc2ncnn12 [MOL:END] [MOL:START] CNCCN [MOL:END] [RXN:8] [MOL:START]
CN(CCN)C(=O)c1cccc2ncnn12 [MOL:END] [MOL:START] O=C(O)CC1CCC2(CC1)CCC20 [MOL:END] [RXN:8] [END]
```

An example synthetic pathway of CSCCC(C)(C)C(=O)N1CC2(CC(NC(=O)c3ncnc4nc[nH]c34)C2)C1 (the right one in Figure 6) is as follows:

```
[START] [MOL:START] CC(C)(C)OC(=O)N1CC2(CC(N)C2)C1 [MOL:END] [RXN:84] [MOL:START] NC1CC2(CNC2)C1
[MOL:END] [MOL:START] O=C(O)c1ncnc2nc[nH]c12 [MOL:END] [RXN:8] [MOL:START]
O=C(NC1CC2(CNC2)C1)c1ncnc2nc[nH]c12 [MOL:END] [MOL:START] CSCCC(C)(C)C(=O)O [MOL:END] [RXN:8]
[END]
```

Here, tokens for *building blocks*, *reactions*, and *intermediates* are indicated by colors.

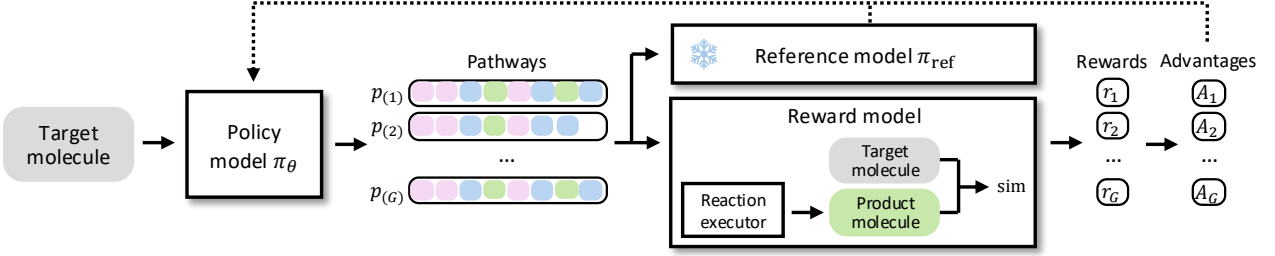


Figure 5 | RL finetuning of ReaSyn using the GRPO algorithm.

## C.2. Model Architecture

We adopt the standard encoder-decoder Transformer architecture following Gao et al. [16]. Specifically, the encoder of ReaSyn has 6 layers, with a hidden dimension of 768, 16 attention heads, a feed-forward dimension of 4096, and the maximum sequence length of 256. The decoder of ReaSyn has 10 layers, with a hidden dimension of 768, 16 attention heads, a feed-forward dimension of 4096, and the maximum sequence length of 768. Overall, ReaSyn has a total of 166,552,848 parameters. Note that ReaSyn has fewer parameters than SynFormer [16] of 229,935,480 parameters, because ReaSyn does not need extra heads for fingerprint diffusion and reaction classification.

## D. Details on Training

In our paper, following [16], we used the set of 115 reactions that include common uni-, bi- and tri-molecular reactions, and the set of 211,220 purchasable building blocks in the Enamine’s U.S. stock catalog [10] curated by Gao et al. [16]<sup>2</sup>.

### D.1. Supervised Learning

Given the sets of building blocks and reactions, the dataset of  $\mathbf{p}$  can be generated on-the-fly during training by iteratively executing compatible reactions to random building blocks. A stack is maintained for each pathway to keep track of intermediate products during data generation, and the corresponding token blocks of reactants, reaction rules, and products are concatenated to construct a sequence in the CoR notation, following Eq. (2). ReaSyn is trained using the AdamW optimizer [33] with a learning rate of  $3e-4$  for 500k steps. A batch size per GPU was set to 64, and 16 NVIDIA A100 GPUs were used. The training took about 5 days.

### D.2. RL Finetuning

After the model is trained with the supervised learning stage, an RL finetuning can be performed to further enhance the model’s reasoning capability. As shown in Figure 5, using the GRPO algorithm [43], the trained model  $\pi_\theta$  first generates a group of pathways  $\{\mathbf{p}_{(i)}\}_{i=1}^G$  given the target molecule  $\mathbf{x}$ , where  $G$  is the group size. The reward  $r_i$  of  $\mathbf{p}_{(i)}$  is calculated as the pairwise similarity between the input target molecule  $\mathbf{x}$  and the generated product molecule  $\text{prod}(\mathbf{p}_{(i)})$ . Then, the advantage  $A_i$  of  $\mathbf{p}_{(i)}$  is calculated as follows:

$$A_i := \frac{r_i - \text{mean}(\{r_i\}_{i=1}^G)}{\text{std}(\{r_i\}_{i=1}^G)}, \quad (5)$$

where  $\text{mean}$  and  $\text{std}$  denote the mean and standard operation, respectively.

Using the dataset  $\mathcal{D}_{\text{RL}}$  composed of  $\mathbf{x}$ , the model  $\pi_\theta$  is trained with the following loss function:

$$\mathcal{L}_{\text{RL}} = -\mathbb{E}_{\mathbf{x} \sim \mathcal{D}_{\text{RL}}, \{\mathbf{p}_{(i)}\}_{i=1}^G \sim \pi_\theta(\mathbf{p}|\mathbf{x})} \left[ \frac{1}{G} \sum_{i=1}^G \left\{ \min \left[ \frac{\pi_\theta(\mathbf{p}_{(i)}|\mathbf{x})}{\pi_{\theta_{\text{old}}}(\mathbf{p}_{(i)}|\mathbf{x})}, \text{clip} \left( \frac{\pi_\theta(\mathbf{p}_{(i)}|\mathbf{x})}{\pi_{\theta_{\text{old}}}(\mathbf{p}_{(i)}|\mathbf{x})}, 1 - \epsilon, 1 + \epsilon \right) A_i \right] - \beta \mathbb{D}_{\text{KL}}[\pi_\theta || \pi_{\text{ref}}] \right\} \right], \quad (6)$$

<sup>2</sup><https://github.com/wenhao-gao/synformer> (Apache-2.0 license)

where  $\epsilon$  and  $\beta$  are hyperparameters and  $\pi_{\text{ref}}$  is the frozen reference model at the beginning of the RL finetuning stage. In practice, we applied the clipping to the log space to avoid overflow, i.e.,  $\text{clip}(\log \pi_{\theta}(\mathbf{p}_{(i)}|\mathbf{x}) - \log \pi_{\theta_{\text{old}}}(\mathbf{p}_{(i)}|\mathbf{x}), -\epsilon', \epsilon')$  before applying the exponentiation.

Since the purpose of the RL finetuning stage is to enhance the pathway diversity by allowing the model to explore different reasoning paths that yield the same end product, only multi-step pathways, i.e., pathways with the number of steps  $\geq 2$ , were used as the training data. ReaSyn is finetuned using the AdamW optimizer [33] with a learning rate of  $1e-5$  for 1k steps.  $\epsilon'$  was set to 0.2 and  $\beta$  was set to  $1e-4$ . A batch size per GPU was set to 2 with a gradient batch accumulation of 4, and 4 NVIDIA A100 GPUs were used. The training took about 5 hours.

## E. Details on Inference

Inference of ReaSyn was implemented similarly to the official codebase<sup>3</sup> of Gao et al. [16]. Specifically, the Transformer decoder of ReaSyn autoregressively generates a pathway block-by-block, and a stack is maintained for each pathway  $\mathbf{p}$  being generated. If the generated block  $\mathbf{p}^b$  corresponds to a molecule, a building block is retrieved from the building block library by conducting the nearest-neighbor search, and then pushed to the stack. Here, the nearest-neighbor search used the following similarity function:

$$\text{sim}(\mathbf{x}, \mathbf{x}') = \frac{1}{\text{dist}(\mathbf{x}, \mathbf{x}') + 0.1}, \quad (7)$$

where  $\text{dist}(\mathbf{x}, \mathbf{x}')$  is the 1-norm distance between the Morgan fingerprints [37] (radius 2, length 2048) of  $\mathbf{x}$  and  $\mathbf{x}'$ . If the generated block  $\mathbf{p}^b$  is a reaction, the required number of reactants are popped from the top of the stack, then the reaction is executed using the RDKit [29] library. Unlike in Gao et al. [16], if the predicted reaction is incompatible with the reactants in the current stack, ReaSyn chooses the next reaction with the next highest prediction logit. The resulting intermediate product is pushed back to the stack and is also appended as a block to  $\mathbf{p}$ . To extensively explore the synthesizable chemical space with multiple synthesizable analog suggestions, beam search is employed. All experiments were conducted using 4 NVIDIA A100 GPUs.

### E.1. Synthesizable Molecule Reconstruction

In the synthesizable molecule reconstruction experiments, a search width of 12, an exhaustiveness of 32, the maximum evolution step of 8 were used during the search. Similarity in Table 1 and similarity (Morgan) in Table 2 are measured as the Tanimoto similarity on the Morgan fingerprint [37] with radius 2 and length 4096. Note that ChemProjector [36] in Table 2 used a search width of 24 and an exhaustiveness of 64, which are more generous settings than the other methods.

### E.2. Synthesizable Goal-directed Molecular Optimization

In the synthesizable goal-directed molecular optimization experiments, a search width of 2, an exhaustiveness of 4, the maximum evolution step of 8 were used during the search. The rate of the mutation operation of Graph GA was set to 0.1. The reward model used in the goal-directed search was implemented as a single-layer MLP that takes the Morgan fingerprints with radius 2 and length 1024 as input and predicts the target chemical property. The reward model was trained on-the-fly during inference, after every reproduction step of Graph GA-ReaSyn. The mean squared error (MSE) loss was used to train the reward model.

In Table 3, the learning rate to train the reward model was set using the search space  $\{1e-3, 1e-4, 5e-5, 1e-5\}$  for each oracle function. A population size of 100 and an offspring size of 100 were used. Following Gao et al. [15] and Sun et al. [46], the maximum number of oracle calls was set to 10k the optimization performance was evaluated with the area under the curve (AUC) of the top-10 average score versus oracle calls.

In Table 4, the learning rate to train the reward model was set to  $1e-5$ . A population size of 400 and an offspring size of 100 were used. The objective function to optimize is set to  $\text{sEH score} \cdot \widehat{\text{SA}} \cdot \widehat{\text{QED}}$ , where  $\text{sEH}$

<sup>3</sup><https://github.com/wenhao-gao/synformer> (Apache-2.0 license)

Table 9 | **Reconstruction rate (%) results in synthesizable molecule reconstruction.** The results are the means and the standard deviations of 3 runs. The best results are highlighted in bold.

Method	Dataset		
	Enamine	ChEMBL	ZINC250k
AiZynthFinder [18]	$34.0 \pm 0.3$	<b><math>55.1 \pm 0.1</math></b>	$11.4 \pm 0.1$
ReaSyn (ours)	<b><math>76.8 \pm 0.7</math></b>	$21.9 \pm 0.2$	<b><math>41.2 \pm 0.2</math></b>

score is the normalized binding affinity of the sEH protein target predicted by a proxy model [1], and  $\widehat{\text{SA}}$  and  $\widehat{\text{QED}}$  are normalized SA score [11] and QED [2] defined as:

$$\widehat{\text{SA}} = \frac{10 - \text{SA}}{9} \in [0, 1], \quad \widehat{\text{QED}} = 2 \cdot \text{clip}(\text{QED}, 0, 0.5) \in [0, 1]. \quad (8)$$

Note that in Table 4, the baselines used a total of 300k oracle calls and the average values of 1k generated molecules were reported. In contrast, Graph GA-ReaSyn used only 5k oracle calls and the average values of top-1k generated molecules generated among the 5k molecules were reported, showing very high sampling efficiency compared to the baselines.

### E.3. Synthesizable Hit Expansion

In the synthesizable hit expansion experiment, a search width of 12 and an exhaustiveness of 128 were used to collect 100 synthesizable analogs for each input molecule. The oracle function that computes the JNK3 inhibition score [22] was used as the goal-directed reward model that guides the search.

## F. Additional Experimental Results

### F.1. Comparison with Retrosynthesis Planning Method

Assuming all input molecules are synthesizable, the synthesizable analog generation problem can be applied to the problem of retrosynthesis planning. Since the pathways that successfully reconstruct a given input molecule in synthesizable analog generation correspond to the solved pathways in retrosynthesis planning, we compare the reconstruction rates of ReaSyn with those of a state-of-the-art retrosynthesis planning method in Table 9. AiZynthFinder [18] is an MCTS-based method that recursively breaks down a given product molecule into reactant molecules to find pathways to building blocks. Note that it uses 42,554 reaction templates extracted from the USPTO reaction set [34] and 17,422,831 building blocks from the ZINC stock [23], so its solution space is much larger than that of ReaSyn, which is defined by 115 reactions and 211,220 building blocks in this paper. We used the official codebase<sup>4</sup> to run AiZynthFinder.

As shown in the table, ReaSyn shows higher reconstruction rate on the Enamine and ZINC250k test sets and lower reconstruction rate on the ChEMBL test set. We suspect that this is because the synthesizable space of AiZynthFinder is more in line and compatible with the ChEMBL test set than that of ReaSyn. Nevertheless, ReaSyn outperforms AiZynthFinder by a large margin in the other two test sets, despite its much smaller design space. Moreover, we emphasize that the synthesizable analog generation approach is much more versatile. Only reconstruction rate can be measured using retrosynthesis planning methods, and they cannot be applied to other tasks, such as suggesting synthesizable analogs given unsynthesizable molecules, goal-directed optimization of the end products, or synthesizable hit expansion.

<sup>4</sup><https://github.com/MolecularAI/aiynthfinder> (MIT license)

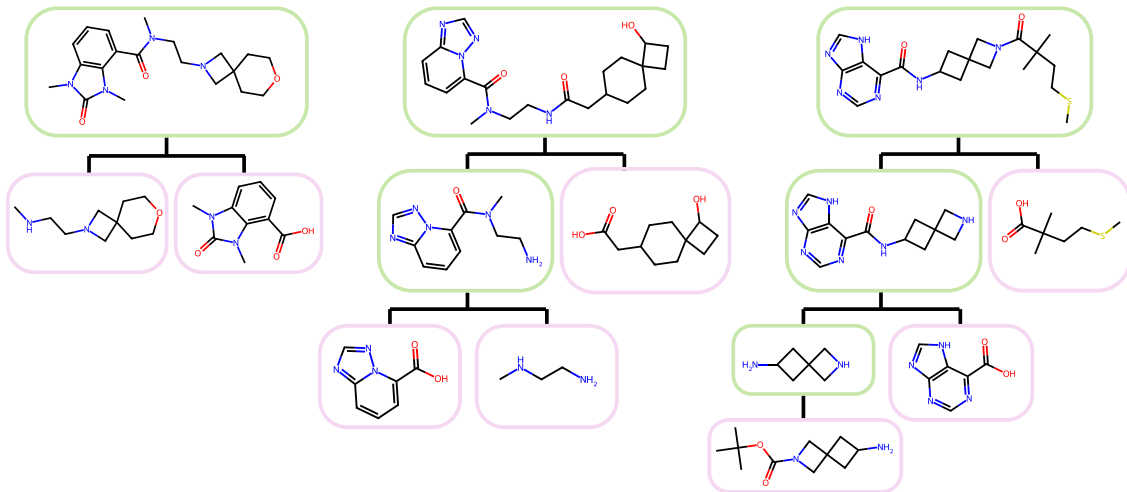


Figure 6 | **Examples of synthetic pathways generated** by ReaSyn in synthesizable molecule reconstruction of Enamine molecules.

## F.2. Generated Examples

We provide examples of reconstructed Enamine molecules in synthesizable molecule reconstruction in Figure 6. We also provide additional examples of hit molecules and generated synthesizable analogs in JNK3 hit expansion in Figure 7.

Hit molecule	Synthesizable analogs				
					
JNK3 score = 0.68	JNK3 score = 0.73 sim = 0.850	JNK3 score = 0.72 sim = 0.946	JNK3 score = 0.72 sim = 0.756	JNK3 score = 0.71 sim = 0.791	JNK3 score = 0.71 sim = 0.705
					
JNK3 score = 0.67	JNK3 score = 0.67 sim = 0.971	JNK3 score = 0.64 sim = 0.872	JNK3 score = 0.64 sim = 0.850	JNK3 score = 0.54 sim = 0.971	JNK3 score = 0.54 sim = 0.971
					
JNK3 score = 0.66	JNK3 score = 0.42 sim = 0.630	JNK3 score = 0.42 sim = 0.605	JNK3 score = 0.42 sim = 0.613	JNK3 score = 0.42 sim = 0.622	JNK3 score = 0.41 sim = 0.605
					
JNK3 score = 0.62	JNK3 score = 0.58 sim = 0.671	JNK3 score = 0.57 sim = 0.804	JNK3 score = 0.55 sim = 0.519	JNK3 score = 0.54 sim = 0.476	JNK3 score = 0.51 sim = 0.464
					
JNK3 score = 0.55	JNK3 score = 0.64 sim = 0.800	JNK3 score = 0.63 sim = 0.786	JNK3 score = 0.63 sim = 0.786	JNK3 score = 0.61 sim = 0.833	JNK3 score = 0.60 sim = 0.786
					
JNK3 score = 0.51	JNK3 score = 0.63 sim = 0.594	JNK3 score = 0.62 sim = 0.569	JNK3 score = 0.60 sim = 0.608	JNK3 score = 0.59 sim = 0.585	JNK3 score = 0.51 sim = 0.829
					
JNK3 score = 0.50	JNK3 score = 0.68 sim = 0.723	JNK3 score = 0.68 sim = 0.723	JNK3 score = 0.58 sim = 0.790	JNK3 score = 0.58 sim = 0.790	JNK3 score = 0.53 sim = 0.667
					
JNK3 score = 0.50	JNK3 score = 0.79 sim = 0.704	JNK3 score = 0.79 sim = 0.691	JNK3 score = 0.79 sim = 0.691	JNK3 score = 0.78 sim = 0.704	JNK3 score = 0.71 sim = 0.593
					
JNK3 score = 0.49	JNK3 score = 0.69 sim = 0.684	JNK3 score = 0.68 sim = 0.672	JNK3 score = 0.68 sim = 0.650	JNK3 score = 0.68 sim = 0.672	JNK3 score = 0.68 sim = 0.736
					
JNK3 score = 0.49	JNK3 score = 0.51 sim = 0.651	JNK3 score = 0.50 sim = 0.750	JNK3 score = 0.48 sim = 0.774	JNK3 score = 0.48 sim = 0.660	JNK3 score = 0.47 sim = 0.800

Figure 7 | Examples of hit molecules and generated synthesizable analogs by ReaSyn in JNK3 hit expansion. JNK3 inhibition score measured by the JNK3 proxy and similarity to the input hit are provided at the bottom of each generated analog.